Supplementary Information (SI) for RSC Applied Interfaces.

Electrocatalytic Oxidation of Methanol: Role of Thorium (Th) Doping in $MoSe_2$

Pooja[a], Sarita Yadav[a], Ravinder Pawar*[a], Rajeev Ahuja*[b,c]

[a] *Laboratory of Advanced Computation and Theory for Materials and Chemistry (LACTMC), Department of Chemistry, National Institute of Technology Warangal (NITW), Warangal, Telangana-506004, India.*

Email: ***ravinder_pawar@nitw.ac.in***

[b] Condensed Matter Theory, Department of Physics and Astronomy, Uppsala University, Uppsala, 75120, Sweden

[c] Department of Physics, Indian Institute of Technology Ropar, Punjab, India

Email: ***rajeev.ahuja@physics.uu.se***

Computational details

The change in Gibbs free energy (ΔG) for each reaction step was calculated using Nørskov et al. method.[1] Under experimental conditions (U = 0, pH, pressure = 1 bar, temperature = 298 K), the free energy ΔG is calculated as follows:

$$\Delta G = \Delta E + \Delta ZPE - T\Delta S + \Delta G_U + \Delta G_{pH}, \quad \text{(S1)}$$

here, ΔE is the reaction energy of the reactant and product adsorbed on the catalyst surface, derived from DFT analysis. The changes in zero-point energy (ΔZPE) and entropy (ΔS) for the reaction are also considered. ΔG_{pH} accounts for the pH correction, calculated as $\Delta G_{pH} = -k_B T ln[H^+] = 0.0593pH$ when the pH is not zero.

The onset potentials were computed using the computational standard hydrogen electrode method, which accounts for the applied potential (U) by incorporating the term $\Delta G_U = -eU$ to into the free energy calculation for proton-electron pair formation. The electrochemical potential for each step was then determined as $\Delta U_i = \Delta G_i/e$, where ΔG_i represents the reaction free energy. Finally, the overall onset potential was estimated as $U_{onset} = max(\Delta G_i/e)$, yielding the maximum value of the electrochemical potential.[1]

Periodic Energy Decomposition Analysis using SCM-ADF

The optimized geometries obtained by employing GGA-PBEsol level of calculation were taken in consideration to probe the nature of interaction between two fragments including catalyst (fragment A) and methanol (fragment B) using energy decomposition analysis (EDA).[2–4] This method is helpful to analyze the interaction energy between the two fragments of the molecule into well-defined parameters, like electrostatic interaction (E_{elstat}), orbital interaction (E_{orb}), and Pauli repulsion (E_{Pauli}) energies. The calculations were performed using Slater type orbitals (STOs) enclosing double-ξ polarization (DZP) basis set without any frozen core approximation.[5] All the calculation were performed using Amsterdam density functional theory (ADF) program package.

In addition, the attractive E_{elstat} energy corresponds to the classic electrostatic interaction of unperturbed charge distribution of the fragments. E_{Pauli} is an energy change associated with transformation from superposition of unperturbed wave functions of the isolated fragments to the wave function $\Psi_0 = N\hat{A}[\Psi_A\Psi_B]$ which obeys the Pauli principle due to explicit antisymmetrization and renormalization of the product wave function. ΔE_{orb}

explains the polarization and charge transfer effects. The decomposition of total interaction energy (E_{int}) into various components mathematically given as follows:

$$E_{int} = E_{elstat} + E_{orb} + E_{Pauli} \quad \text{(S2)}$$

Characterization

Various characterization techniques were utilized to ensure the successful formation of the prepared Th-doped $MoSe_2$ catalysts. PXRD studies were conducted to investigate phase purity and crystal structure. These studies were performed using Panalytical's X'Pert Pro diffractometer with CuKα radiation over a scan range (2θ) of 20° to 80°. The structural, morphological, and elemental composition of the synthesized catalysts were examined using FESEM with a JEOL JSM IT-800 instrument. Additionally, EDS and elemental mapping were carried out using an accessory integrated into the FESEM instrument. XPS was employed for further analysis using a PHI 5000 Versa Probe III XPS Spectrometer. To analyze the stretching frequency of the synthesized Th-doped $MoSe_2$ catalyst, FT-IR was conducted using a Perkin Elmer instrument. The FT-IR scan range covered from 4000 to 400 cm^{-1}, providing detailed insights into the molecular structure and bonding characteristics. Brunauer−Emmett−Teller (BET) was conducted on Quantachrome Autosorb IQ-MP Instrument.

Electrochemical Analysis

The MOR measurements were conducted using a *MedPstat* electrochemical analyzer equipped with a three-electrode system. An Ag/AgCl electrode served as the reference electrode, while a Pt electrode was employed as the counter electrode. The catalyst ink was prepared by dispersing 2.0 mg of catalyst in a mixture comprising 200 μL of isopropanol and 10 μL of Nafion (5%). Subsequently, the ink was ultrasonicated for 30 minutes to ensure a homogeneous dispersion of the catalyst. The resulting ink was then deposited onto the surface of a glassy carbon (GC) electrode with a diameter of 5 mm and air-dried. Liquid analyte analysis was carried out using ^{1}HNMR on a Bruker Avance-III 400 MHz NMR spectrometer using $CDCl_3$ as a solvent. For the Tafel equation, $\eta = a + b\log(j)$, where η is the overpotential, b is the Tafel slope, and j is the current density. It was fitted in the Tafel range. The electrochemical impedance spectra (EIS) were recorded at the frequency range from 1000 kHz to 10 mHz in 0.5 M H_2SO_4 + 0.5 M CH_3OH solution with 12 points per decade. The amplitude of the sinusoidal potential signal was 0.49V. The chronoamperometry (CA) experiment of MOR was tested for 20 h in a 0.5 M H_2SO_4 + 0.5 M CH_3OH solution. In the CO stripping experiments, the electrode was first immersed in 0.5 M H_2SO_4 and subjected to N_2 gas purging

for 30 minutes to remove any dissolved oxygen. Next, CO gas was introduced for 1 hour, allowing the CO molecules to adsorb onto the active sites of the electrocatalyst. Finally, N_2 gas was used again to purge the solution, eliminating any dissolved CO. The CO stripping curve was performed in 0.5 M H_2SO_4 solution at a scan rate of 50 mV s^{-1}.

The Mass activity for the NCO catalyst is calculated using the following equation:

$$M_A = J_k / M_{catalyst} \quad \text{(S3)}$$

Where, $J_k = (J_L * J_P)/(J_L - J_P)$

M_A= Mass activity

J_P= Current density at the particular potential

J_L= Highest diffusion limiting current density

$M_{catalyst}$= Catalyst loading (0.005 mg)

The electrochemical active surface area (ECSA) was determined from the electrochemical double-layer capacitance (Cdl). To obtain the Cdl values, cyclic voltammograms (CVs) were recorded at various scan rates within the non-faradaic region. By plotting the difference between the anodic and cathodic current densities ($\Delta j = j_a - j_c$) against the scan rates, the Cdl values were derived from the slope of the resulting curve. These Cdl values correspond to half of the linear slope. Assuming a linear relationship between ECSA and Cdl, the following equation was used to calculate the ECSA:

$$\text{ECSA} = Cdl/(Cs\ per\ cm^2) \quad \text{(S4)}$$

The Specific activity (SA) is calculated using the equation:

$$SA = I/ECSA \quad \text{(S5)}$$

The specific activity of Th-doped $MoSe_2$ at 1.02 V vs RHE was calculated by normalizing the oxidation current to the ECSA.

NOTE: *From a radiological safety standpoint, the thorium compound used in this study—thorium nitrate [$Th(NO_3)_4$], is considered safe when handled under standard laboratory conditions. It emits weak alpha particles, which pose minimal external risk but can be hazardous if the material is inhaled or ingested. While thorium has low specific activity due to its long half-life (^{232}Th, ~1.4×10^{10} years), long-term internal exposure must still be avoided to minimize potential health risks. Appropriate safety measures, such as the use of personal protective equipment and working within a fume hood, were strictly followed during all experimental procedures.*

"Prolonged exposure to radioactive materials through ingestion, whether oral or nasal, may lead to adverse health effects and should be strictly avoided".

Band Structure

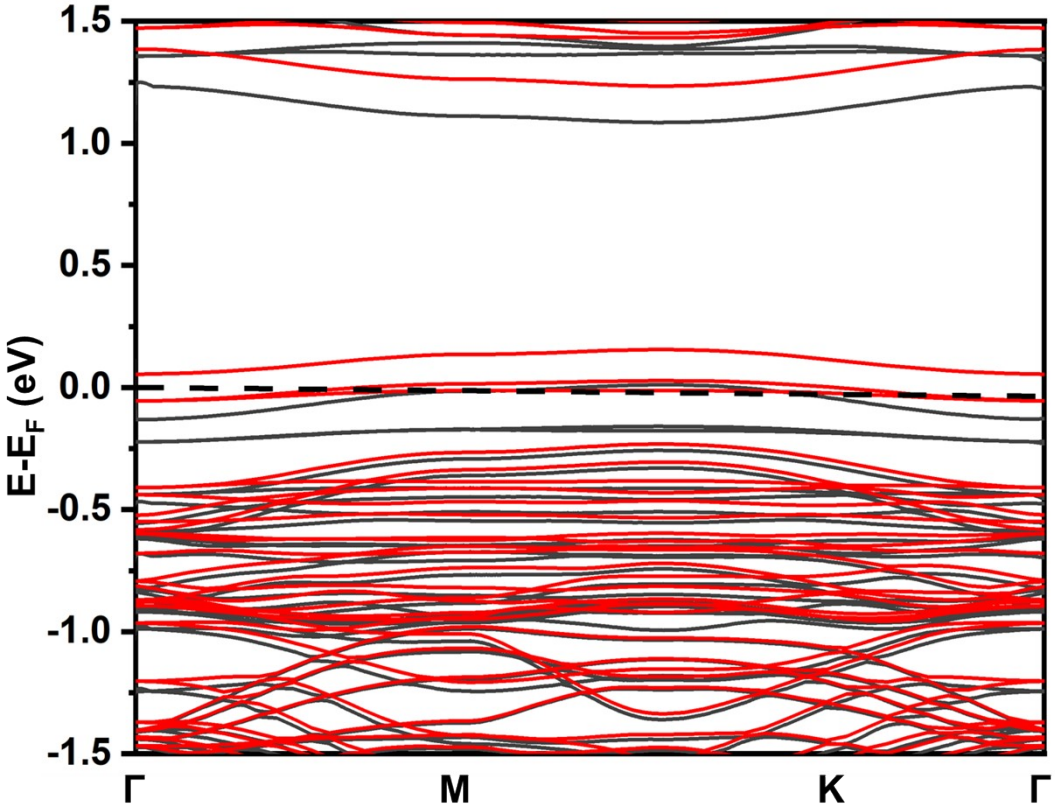

Figure S1. Band structure of Th-doped $MoSe_2$

Elementary Steps in the MOR Involving Electron Transfer, Along With Their Corresponding Reaction Free Energy Expressions and Their Electronic Properties

The MOR was analyzed using individual step-wise reactions as follow:

$$CH_3OH + \rightarrow CH_3O^* / CH_2OH^* + H^+ + e^- \quad \text{(S4)}$$

$$CH_3O^*/CH_2OH^* \rightarrow CH_2O^* + H^+ + e^- \quad \text{(S5)}$$

$$CH_2OH^* \rightarrow CHOH^* + H^+ + e^- \quad \text{(S6)}$$

$$CH_2O^*/CHOH^* \rightarrow CHO^* + H^+ + e^- \quad \text{(S7)}$$

$$CHOH^* \rightarrow COH^* + H^+ + e^- \quad \text{(S8)}$$

$$CHO^*/COH^* \rightarrow CO^* + H^+ + e^- \quad \text{(S9)}$$

The calculation of reaction free energy (ΔG_1,ΔG_2,ΔG_3,ΔG_4) for above mentioned reaction are as follows:

$$\Delta G_1 = G\left(CH_3O^*/CH_2OH^*\right) + 1/2H_2(g) - G(*) - G\left(CH_3OH\right) \quad \text{(S10)}$$

$$\Delta G_2 = G\left(CH_2O^*/CHOH^*\right) + 1/2H_2(g) - G\left(CH_3O^*/CH_2OH^*\right) \quad \text{(S11)}$$

$$\Delta G_3 = G\left(CHO^*/COH^*\right) + H_2(g) - G\left(CH_2O^*/CHOH^*\right) \quad \text{(S12)}$$

$$\Delta G_4 = G\left(CO^*\right) + 1/2H_2(g) - G\left(CHO^*/COH^*\right) \quad \text{(S13)}$$

where, $G = \Delta E + \Delta ZPE - T\Delta S$.

Under the standard hydrogen electrode computation framework, G is estimated by $1/2GH_2(g)$.

Optimised Geometry of Intermediates

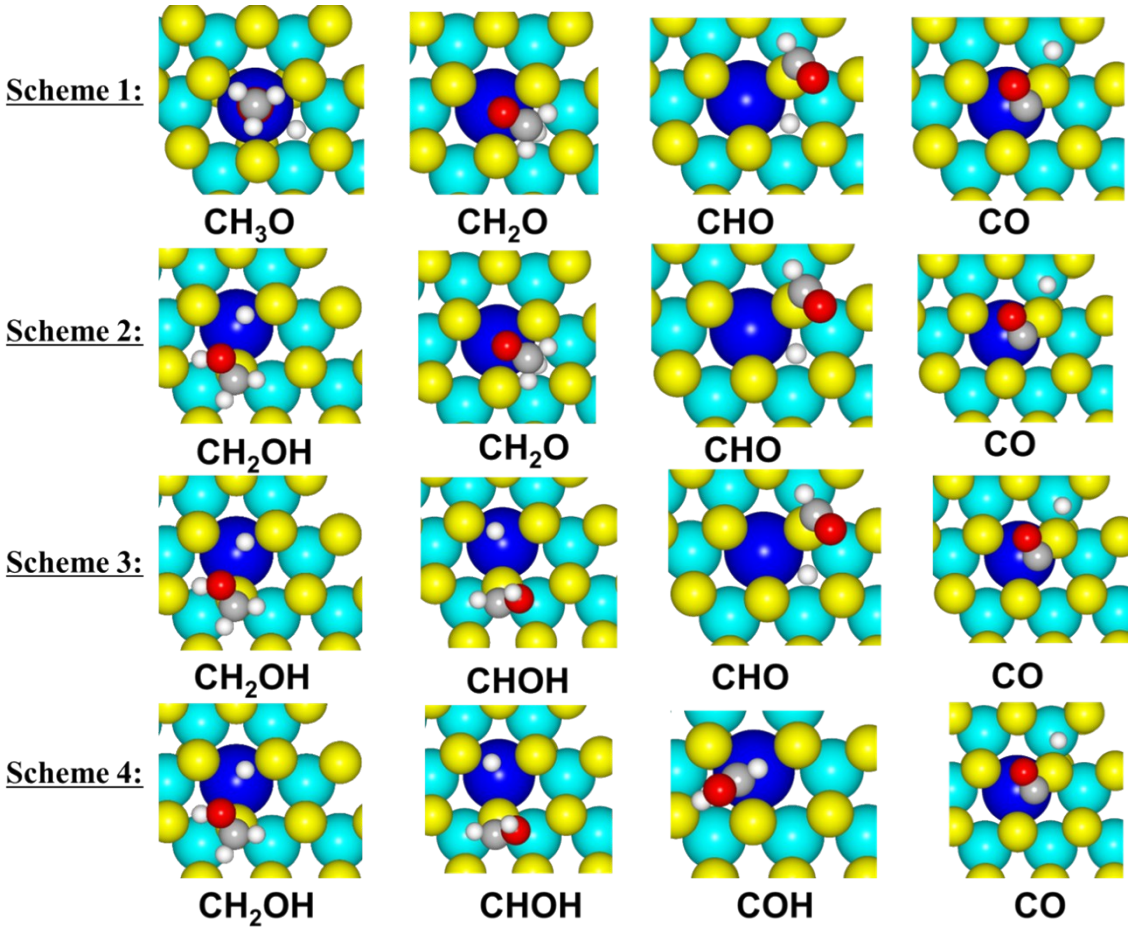

Figure S2. Optimised geometry of various intermediate involving in oxidation of methanol. Color code: Cyan: Mo, Yellow: Se, Blue: Th, Grey: C, Red: O, and white: H

Activation of O-H bond

Scheme 1: $CH_3OH^* \rightarrow CH_3O^* + H^* \rightarrow CH_2O^* + H^* \rightarrow CHO^* + H^* \rightarrow CO^* + H^*$

Scheme 1 shows the O-H bond cleavage in methanol, resulting in the primarily removal of a hydrogen atom from the methylidyne group. The reaction starts with the dehydrogenation of CH_3OH, producing CH_3O and a hydrogen atom. Initially, CH_3OH adsorbs at its most stable site, with the hydroxyl hydrogen positioned near to the Se site (2.70 Å), which is adjacent to the Th-doping. For CH_3OH adsorbed on the catalyst, the O-Th bond distance measures 4.57 Å. Methanol is then converted to CH_3O, releasing a hydrogen atom. Both CH_3O and the hydrogen atom co-adsorb on the catalyst surface in their most stable configuration, with the hydrogen atom situated at a nearest neighbouring site and CH_3O adsorbed through an O side. The distance between O-Th is 2.16 Å. In the next step, dehydrogenation of CH_3O occurs, which results in the formation of CH_2O. During this phase, a hydrogen atom dissociates from the carbon atom in CH_3O and migrates towards the confinement of the Th-doped $MoSe_2$. Similarly, the third step in Scheme 2 involves the dehydrogenation of CH_2O to CHO. The CHO absorbed on top of the Se atom via a C-Se bond with a distance of 2.20 Å.

Activation of the C-H bond

In Schemes 2 to 4, the initial step involves the formation of CH_2OH from methanol, rather than CH_3O. Although the abstraction of a C-H bond in methanol marks the beginning of all these schemes (2 to 4), they diverge in the intermediate responsible for the subsequent dissociation of the hydroxyl hydrogen. Notably, in Scheme 2, the dissociation of the hydroxyl hydrogen occurs from the intermediate CH_2OH. In Scheme 3, it generally dissociates from CHOH. Conversely, Scheme 4 delays the dissociation of the hydroxyl hydrogen until the final dehydrogenation step of COH.

Scheme 2: $CH_3OH^* \rightarrow CH_2OH^* + H^* \rightarrow CH_2O^* + H^* \rightarrow CHO^* + H^* \rightarrow CO^* + H^*$

Scheme 2 initiates with conditions similar to the $CH_3OH^* \rightarrow CH_3O^* + H^*$ step, but with a crucial difference: the hydrogen atom migrates from the C to a neighboring site, resulting in CH_2OH formation. This intermediate then adsorbs onto the catalyst surface, forming a 2.06 Å C-Se bond, contrasting with the O-Se bond in CH_3O formation. The free energy profile reveals that methanol dehydrogenation to CH_2OH is more favorable on the catalyst surface, suggesting that initial C-H cleavage is more likely to occur on this surface. Two potential dehydrogenation pathways for CH_2OH exist: O-H bond scission to form CH_2O (Scheme 2) or C-H bond cleavage to produce CHOH (Scheme 3).

Scheme 3: $CH_3OH^* \rightarrow CH_2OH^* + H^* \rightarrow CHOH^* + H^* \rightarrow CHO^* + H^* \rightarrow CO^* + H^*$

The formation of CHOH involves the breakage of the C-H bond instead of the O-H bond, starting from the most stable CH_2OH configuration. As the reaction proceeds, the carbon-

attached hydrogen atom migrates towards the surface, resulting in CHOH formation, which co-adsorbs with the hydrogen atom on the catalyst surface. Notably, the dehydrogenation of CH_2OH to CHOH is a more efficient process on the catalyst surface due to the strong binding of CHOH and weak adsorption of CH_2O. CHOH can undergo two potential reactions, similar to CH_2OH: conversion to CHO (Scheme 3) or COH (Scheme 4). The final step in Schemes 1, 2, and 3 involves the reaction $CHO^* \rightarrow CO^* + H^*$, where the C-Se bond is nearly perpendicular to the surface, facilitating hydrogen atom activation and transfer to a neighboring site. This leads to the formation of the final products, with CO binding through a C-Se bond and the hydrogen atom co-adsorbing at an adjacent site of the Th-dopant.

Scheme 4: $CH_3OH^* \rightarrow CH_2OH^* + H^* \rightarrow CHOH^* + H^* \rightarrow COH^* + H^* \rightarrow CO^* + H^*$

The reaction proceeds via Scheme 3, culminating in a stable final state where COH adsorbs at the top site of the Se atom. In Scheme 4, COH undergoes further dehydrogenation to yield CO. Initially, COH adsorbs through a C-Se bond (2.22 Å). As the reaction unfolds, the hydrogen atom migrates to a neighbouring site and ultimately binds to the O atom. Notably, CO exhibits enhanced adsorption stability compared to the other schemes, making it a preferred outcome.

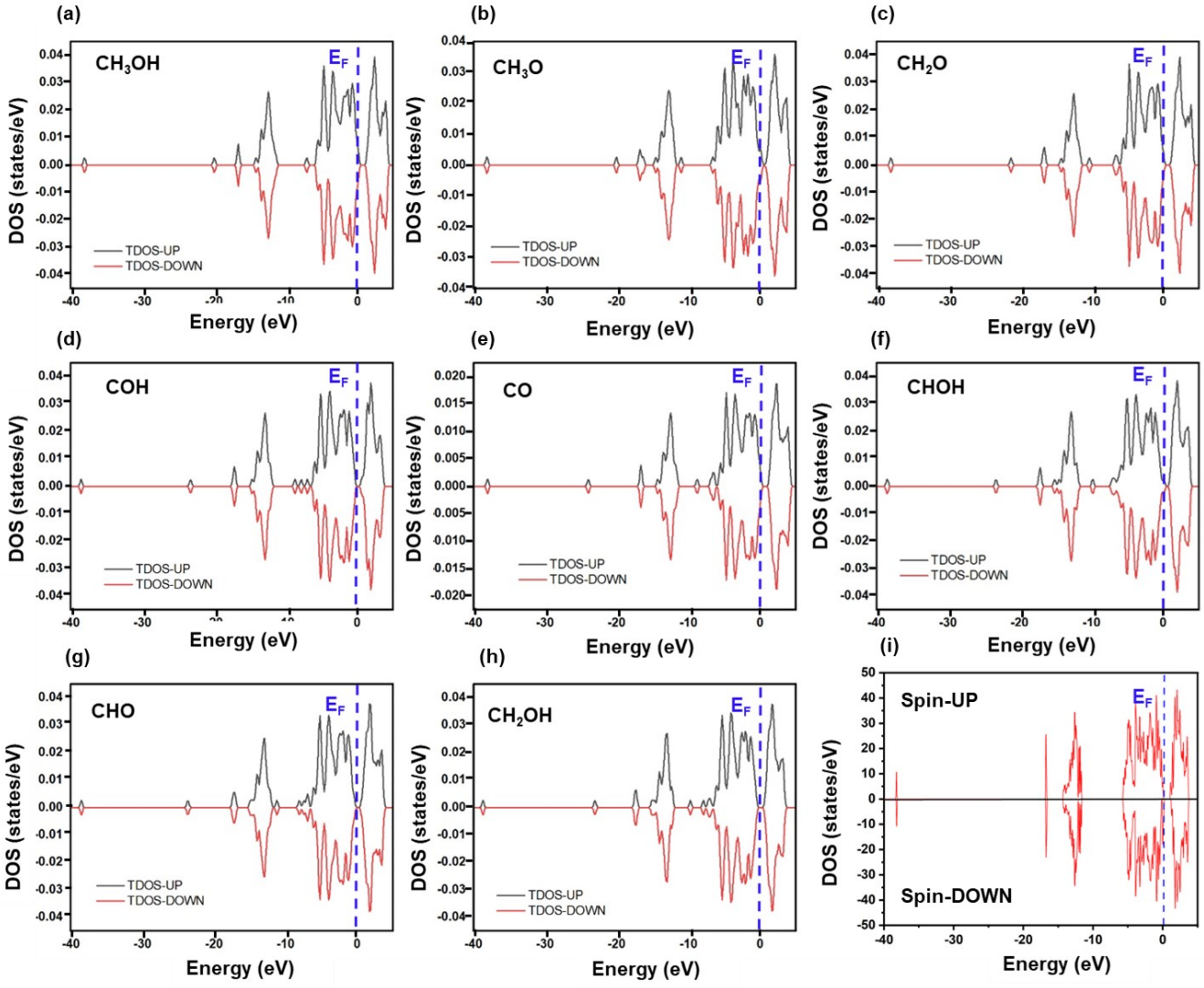

Figure S3. Calculated spin polarized total density of state of important intermediates involving in MOR.

Table S1. Calculated Charges on the Atoms

CH_2OH		CHOH		CHO	
Atom	Mulliken charge	Atom	Mulliken charge	Atom	Mulliken charge
Mo	0.24	Mo	0.25	Mo	0.22
Mo	0.17	Mo	0.16	Mo	0.2
Mo	0.24	Mo	0.25	Mo	0.27

Mo	0.18	Mo	0.18	Mo	0.26
Mo	0.25	Mo	0.25	Mo	0.28
Mo	0.22	Mo	0.22	Mo	0.24
Mo	0.22	Mo	0.22	Mo	0.24
Mo	0.25	Mo	0.24	Mo	0.26
Mo	0.16	Mo	0.16	Mo	0.21
Mo	0.18	Mo	0.16	Mo	0.2
Mo	0.22	Mo	0.23	Mo	0.24
Mo	0.18	Mo	0.17	Mo	0.18
Mo	0.25	Mo	0.24	Mo	0.22
Mo	0.22	Mo	0.22	Mo	0.27
Mo	0.17	Mo	0.15	Mo	0.28
Se	-0.14	Se	-0.12	Se	-0.11
Se	-0.09	Se	-0.09	Se	-0.07
Se	-0.12	Se	-0.15	Se	-0.09
Se	-0.29	Se	-0.11	Se	-0.35
Se	-0.09	Se	-0.29	Se	0
Se	-0.09	Se	-0.09	Se	-0.09
Se	-0.34	Se	-0.33	Se	-0.33
Se	-0.34	Se	-0.34	Se	-0.31
Se	-0.12	Se	-0.11	Se	-0.16
Se	-0.15	Se	-0.15	Se	-0.14
Se	-0.14	Se	-0.15	Se	-0.14
Se	-0.08	Se	-0.09	Se	-0.1
Se	-0.13	Se	-0.13	Se	-0.13
Se	-0.13	Se	-0.13	Se	-0.14
Se	-0.15	Se	-0.15	Se	-0.14
Se	-0.15	Se	-0.12	Se	-0.11
Se	-0.18	Se	-0.16	Se	-0.13
Se	-0.11	Se	-0.12	Se	-0.11
Se	-0.15	Se	-0.11	Se	-0.1
Se	0	Se	0.12	Se	-0.31
Se	-0.14	Se	-0.14	Se	-0.16
Se	-0.15	Se	-0.15	Se	-0.14
Se	-0.15	Se	-0.13	Se	-0.12
Se	-0.12	Se	-0.12	Se	-0.13
Se	-0.08	Se	-0.08	Se	-0.1
Se	-0.11	Se	-0.09	Se	-0.12
Se	-0.09	Se	-0.08	Se	-0.1
Se	-0.08	Se	-0.08	Se	-0.08
Se	-0.34	Se	-0.35	Se	-0.32
Se	-0.1	Se	-0.1	Se	-0.1
Se	-0.13	Se	-0.14	Se	-0.14

Se	-0.09
Th	1.36
C	-0.37
H	0.35
H	0.31
H	-0.07
H	0.53
O	-0.71
Total	0

Se	-0.11
Th	1.42
C	-0.24
H	-0.08
H	0.31
H	0.56
O	-0.69
Total	0

Se	-0.1
Th	1.4
C	0.1
H	0.33
H	-0.3
O	-0.41
Total	0

OCH_3	
Atom	Mulliken charge
Mo	0.21
Mo	0.22
Mo	0.25
Mo	0.25
Mo	0.25
Mo	0.2
Mo	0.26
Mo	0.24
Mo	0.24
Mo	0.21
Mo	0.21
Mo	0.24
Mo	0.25
Mo	0.28
Mo	0.25
Se	-0.08
Se	-0.11
Se	-0.09
Se	-0.15
Se	-0.19
Se	-0.11
Se	-0.22
Se	-0.21
Se	-0.09
Se	-0.14
Se	-0.14
Se	-0.1
Se	-0.13
Se	-0.13
Se	-0.11
Se	-0.09

OCH_2	
Atom	Mulliken charge
Mo	0.23
Mo	0.22
Mo	0.26
Mo	0.28
Mo	0.26
Mo	0.24
Mo	0.25
Mo	0.27
Mo	0.23
Mo	0.22
Mo	0.23
Mo	0.23
Mo	0.25
Mo	0.28
Mo	0.28
Se	-0.09
Se	-0.09
Se	-0.1
Se	-0.32
Se	-0.29
Se	-0.1
Se	-0.34
Se	-0.29
Se	-0.1
Se	-0.14
Se	-0.14
Se	-0.1
Se	-0.14
Se	-0.14
Se	-0.13
Se	-0.09

COH	
Atom	Mulliken charge
Mo	0.24
Mo	0.19
Mo	0.26
Mo	0.19
Mo	0.27
Mo	0.23
Mo	0.21
Mo	0.26
Mo	0.19
Mo	0.2
Mo	0.24
Mo	0.2
Mo	0.25
Mo	0.25
Mo	0.2
Se	-0.1
Se	-0.1
Se	-0.13
Se	-0.08
Se	-0.36
Se	-0.1
Se	-0.32
Se	-0.33
Se	-0.1
Se	-0.14
Se	-0.15
Se	-0.1
Se	-0.13
Se	-0.13
Se	-0.15
Se	-0.13

Se	-0.18
Se	-0.09
Se	-0.08
Se	-0.19
Se	-0.18
Se	-0.14
Se	-0.14
Se	-0.12
Se	-0.11
Se	-0.15
Se	-0.11
Se	-0.11
Se	-0.21
Se	-0.15
Se	-0.13
Se	-0.13
Th	1.58
C	-0.58
H	0.28
H	0.29
H	0.29
H	-0.21
O	-0.91
Total	0

Se	-0.12
Se	-0.09
Se	-0.09
Se	-0.3
Se	-0.13
Se	-0.14
Se	-0.14
Se	-0.14
Se	-0.13
Se	-0.1
Se	-0.13
Se	-0.1
Se	-0.09
Se	-0.28
Se	-0.13
Se	-0.14
Se	-0.12
Th	1.4
C	-0.09
H	-0.28
H	0.28
H	0.27
O	-0.49
Total	0

Se	-0.2
Se	-0.13
Se	-0.13
Se	-0.08
Se	-0.14
Se	-0.14
Se	-0.14
Se	-0.13
Se	-0.1
Se	-0.09
Se	-0.09
Se	-0.09
Se	-0.32
Se	-0.1
Se	-0.13
Se	-0.1
Th	1.37
C	-0.29
H	0.34
H	0.49
O	-0.61
Total	0

CO	
Mo	0.23
Mo	0.21
Mo	0.25
Mo	0.21
Mo	0.25
Mo	0.23
Mo	0.21
Mo	0.25
Mo	0.21
Mo	0.2
Mo	0.2
Mo	0.25
Mo	0.25
Mo	0.25
Mo	0.2
Se	-0.12
Se	-0.09

Se	-0.09
Se	-0.33
Se	-0.2
Se	-0.09
Se	-0.32
Se	-0.33
Se	-0.09
Se	-0.14
Se	-0.14
Se	-0.09
Se	-0.13
Se	-0.13
Se	-0.14
Se	-0.1
Se	-0.12
Se	-0.09
Se	-0.1
Se	-0.31
Se	-0.14
Se	-0.14
Se	-0.13
Se	-0.13
Se	-0.09
Se	-0.12
Se	-0.09
Se	-0.09
Se	-0.33
Se	-0.11
Se	-0.14
Se	-0.11
Th	1.37
C	0.39
H	-0.02
O	-0.4
Total	0

XRD, EDS, and XPS Analysis

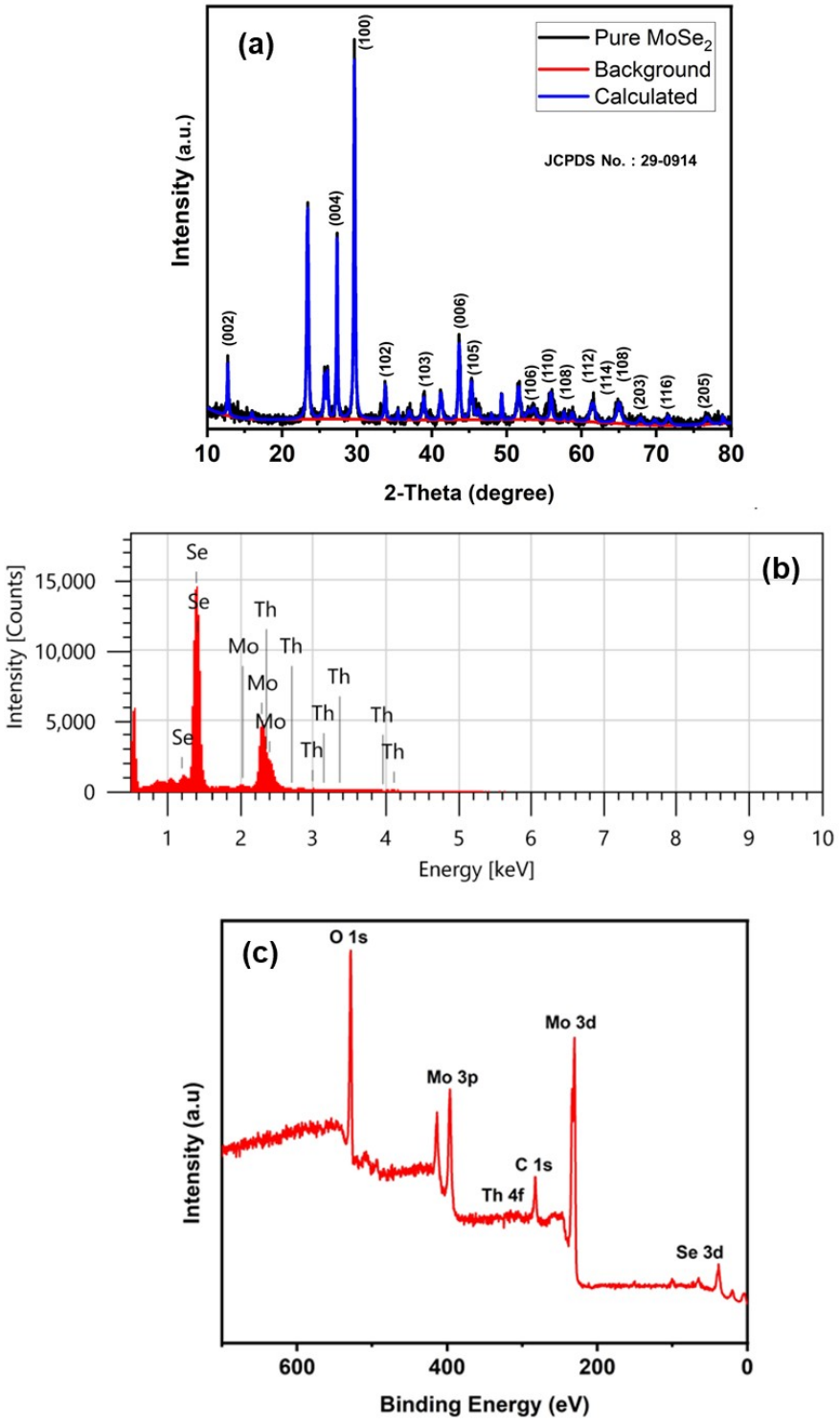

Figure S4. (a) XRD of pure $MoSe_2$, (b) EDS and (c) XPS analysis of Th-doped $MoSe_2$.

Electro-oxidation Of Methanol

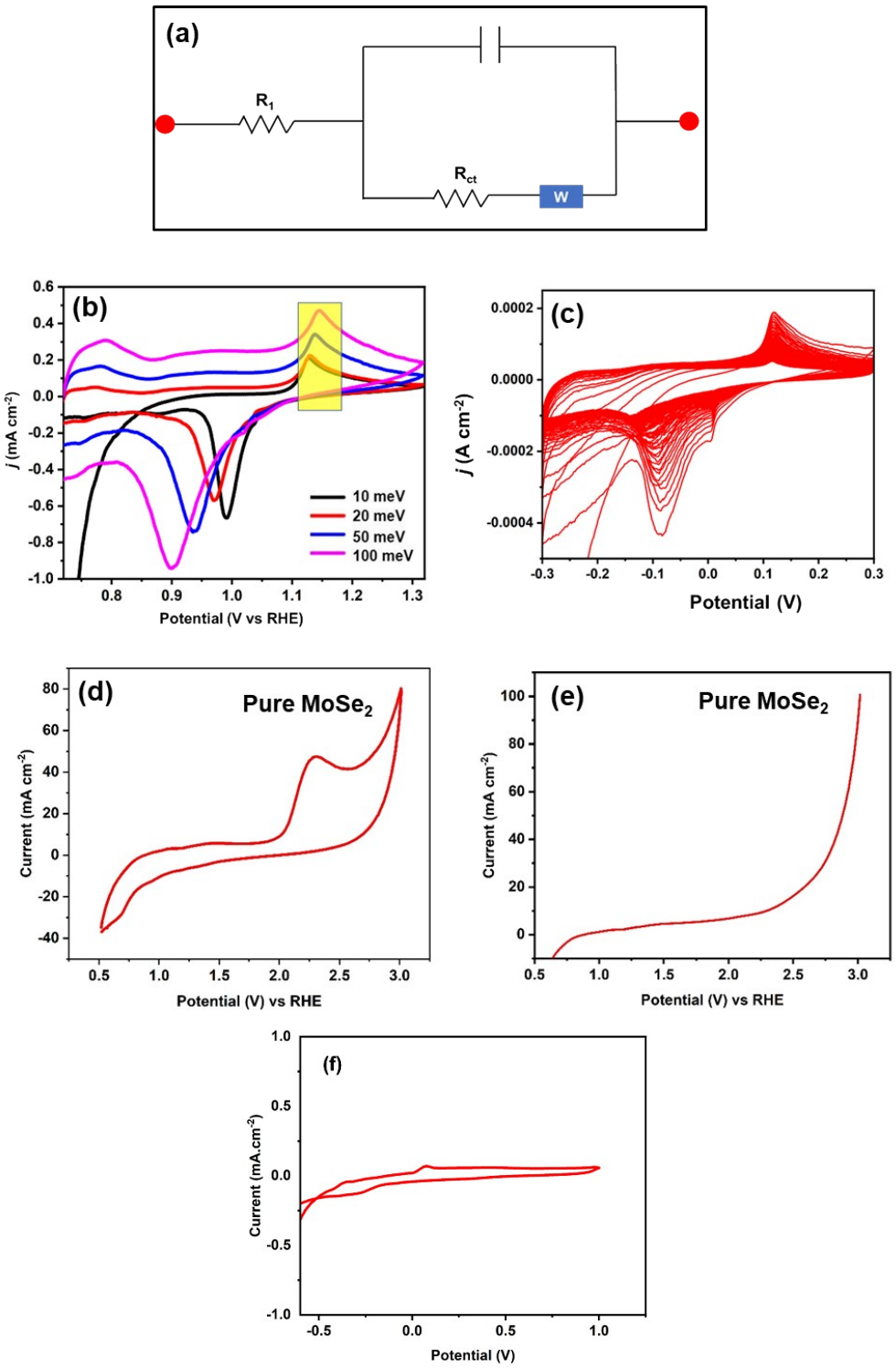

Figure S5. Th-doped $MoSe_2$: (a) fitting circuit model for EIS, (b) CV of 0.5 M H_2SO_4 + 0.5 M CH_3OH solution at a different scan rate versus the RHE, and (c) 100 CV cycles at 0.5 M H_2SO_4 + 0.5 M CH_3OH solution. Pure $MoSe_2$: (d) CV of 0.5 M H_2SO_4 + 0.5 M CH_3OH solution at a 50 mV/s scan rate versus the RHE, and (e) LSV of 0.5 M H_2SO_4 + 0.5 M CH_3OH solution at a 50 mV/s scan rate versus the RHE. (f) Th-doped $MoSe_2$: CV of 0.5 M H_2SO_4

Comparison Between the Synthesised Catalyst with Other Pt-Based Nano-Catalysts

Table S2. Comparison between the synthesised catalyst with other Pt-based nano-catalysts.

(a)

Catalyst	Onset Potential (V)	References
Th-doped $MoSe_2$	1.02	This work
$MoSe_2$	2.50	This work

(b)

S.No.	Catalysts	Electrolyte	Mass activity	References
1	Cubic Pt-Sn alloy nanocrystals	0.5 M H_2SO_4 0.5 M methanol	0.35 A/mg	[6]
2	Ultrathin Pt_3Cu MWs	16 0.5 M H_2SO_4 0.5 M methanol	0.63 A/mg	[7]
3	$Pt_{95}Co_5$ NWs	0.5 M H_2SO_4 1.0 M methanol	0.49 A/mg	[8]
4	PtZn intermetallic NPs	0.5 M H_2SO_4 1.0 M methanol	0.61 A/mg	[9]
5	Popcorn-like PtAu	1 M KOH 1 M methanol	0.60 A/mg	[10]
6	Pt/rGO	0.5 M KOH 0.5 M methanol	0.55 A/mg	[11]
7	PtZn intermetallic NPs	0.1 M KOH 1 M methanol	0.58 A/mg	[9]
8	Pd/DMAB-Ti_3C_2	1.0 M C_2H_5OH + 1.0 M KOH	0.535 A/mg	[12]
9	Pt/gCN	1.0 m CH3OH + 1.0 m H2SO4	0.310 A/mg	[13]
10	Pt/NiCo-LDH	0.5 m CH3OH + 0.1 m NaOH	0.379 A/mg	[14]
11	Pt/IL/NiFeLDH	1.0 m CH3OH + 1.0 m NaOH	0.205 A/mg	[15]
12	Th-doped $MoSe_2$	0.5 M CH_3OH + 0.5M H_2SO_4	0.400 A/mg	This Work

Table S3. Comparison of R_{ct} (Ω) values between the synthesised catalyst with other $MoSe_2$-based nano-catalysts.

Catalyst	R_{ct} (Ω)	References
$MoSe_2$/Rh	10.05	[16]
$MoSe_2$/Rh	18.75	[16]
$MoSe_2$	127.3	[16]
Th-doped $MoSe_2$	1.98	This work

ECSA and CO Stripping Analysis

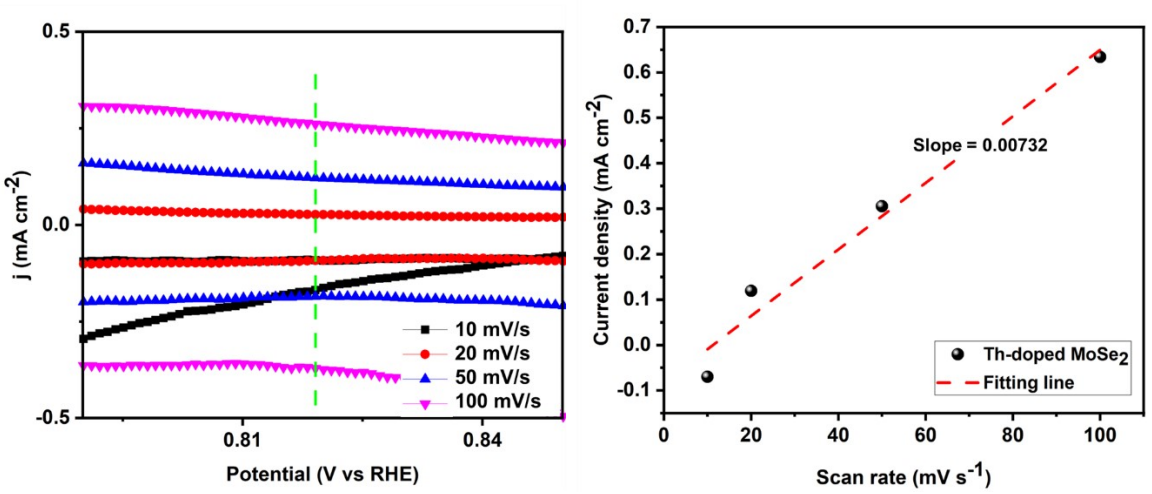

(a)

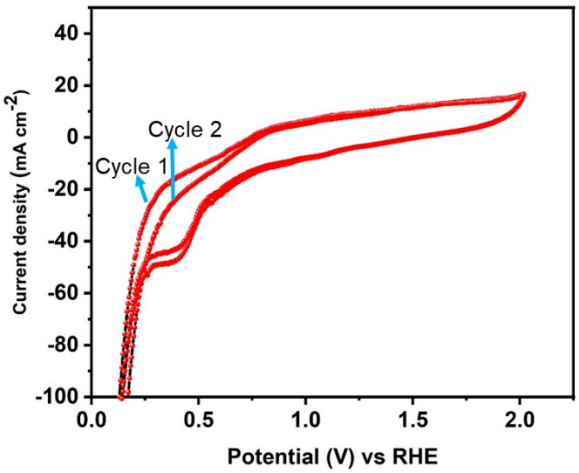

(b)

Figure S6. (a) CV at various scan rates within the non-faradaic region (left), Cdl (right), and (b) CO stripping analysis of Th-doped $MoSe_2$ in 0.5 M H_2SO_4 at a scan rate of 50 mV s^{-1}.

The ECSA of Th-doped $MoSe_2$ was determined to be 0.75 cm^2, and the corresponding SA for methanol oxidation was calculated as 0.027 mA cm^{-2}, reflecting the intrinsic catalytic performance of the material.

^{13}C NMR

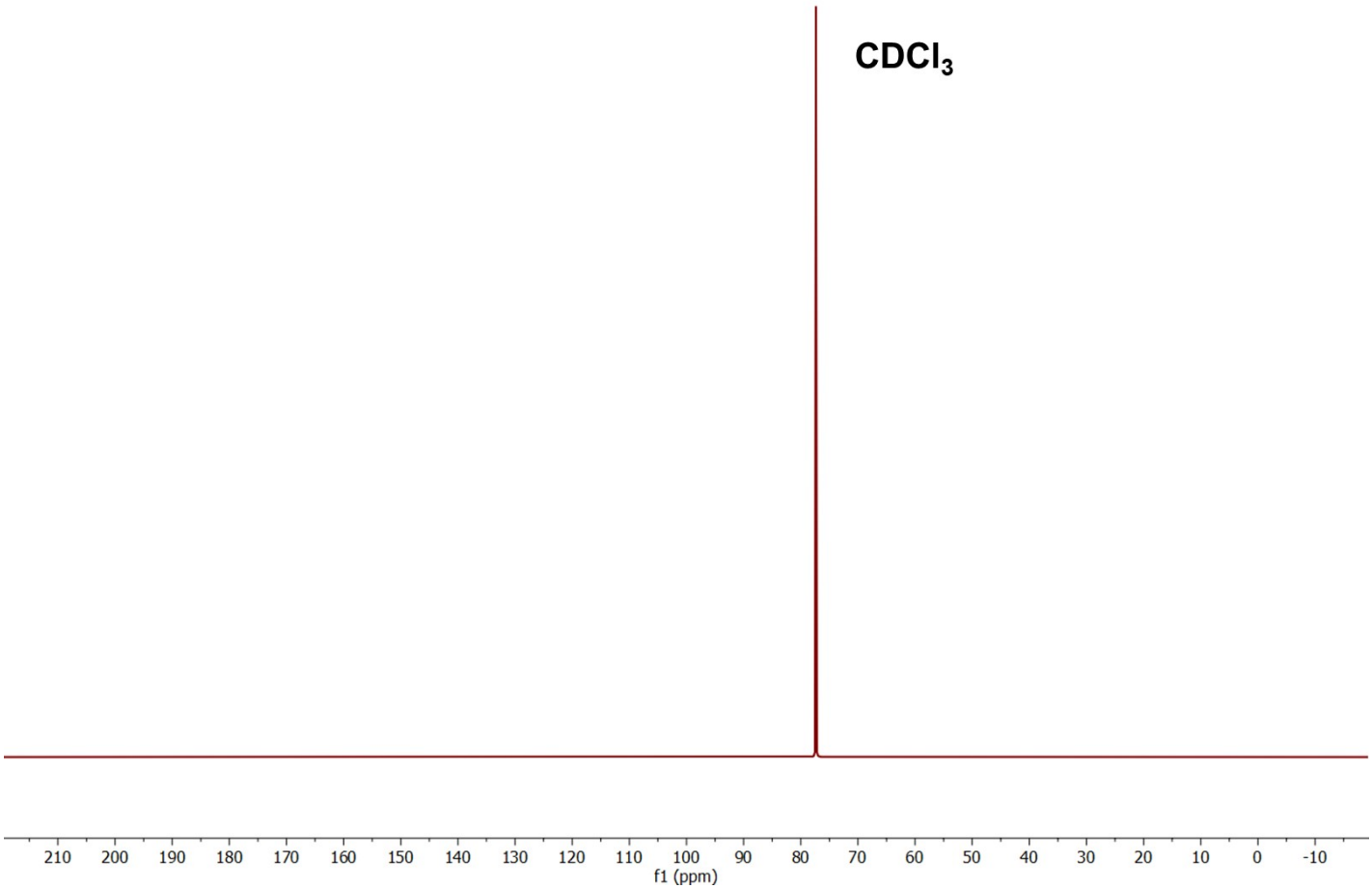

Figure S7. ^{13}C NMR of electrolyte after catalysis onto the surface of Th-doped $MoSe_2$. The ^{13}C NMR is recorded in 0.5 M CH_3OH and 0.5 M H_2SO_4 medium after catalysis.

[1]H-NMR

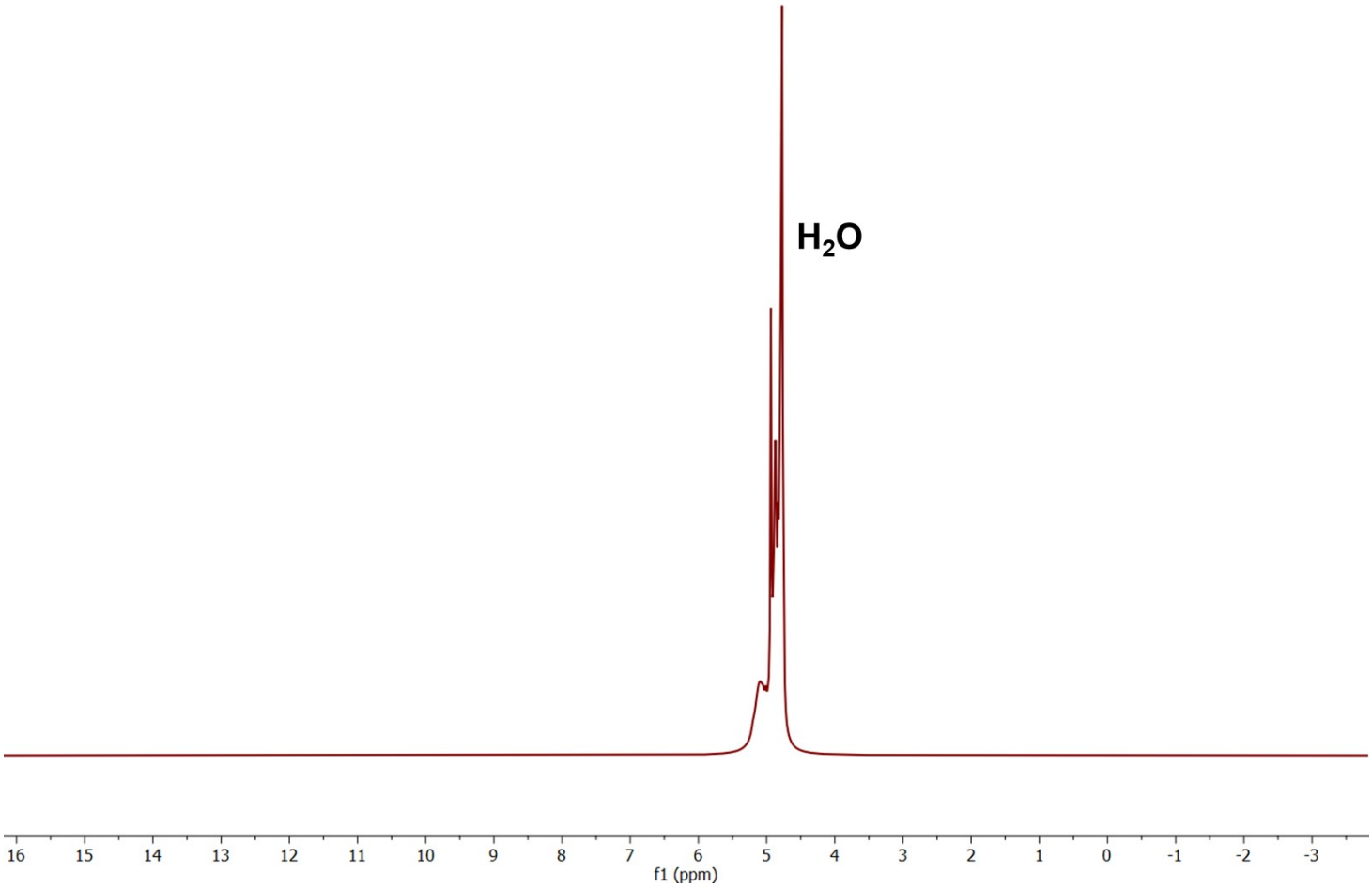

Figure S8. [1]H-NMR of electrolyte after catalysis onto the surface of Th-doped $MoSe_2$. The [1]H-NMR is recorded in 0.5 M CH_3OH and 0.5 M H_2SO_4 medium after catalysis.

FTIR Analysis

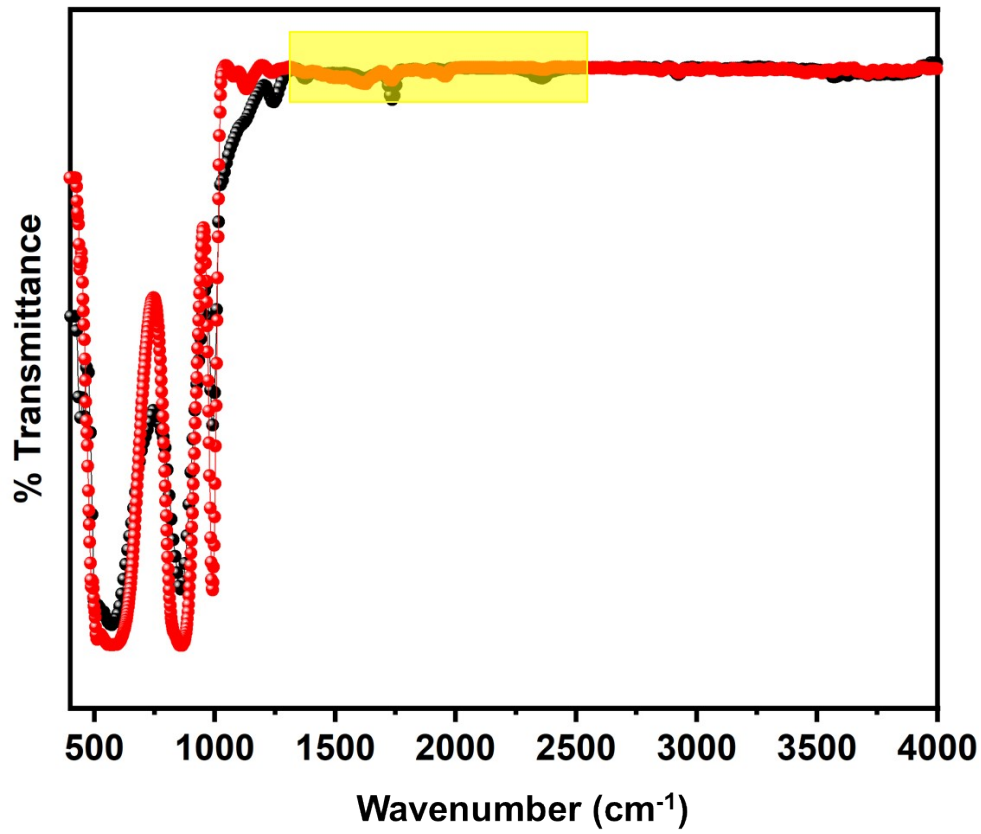

Figure S9. FTIR of electrocatalyst before (black) and after (red) the electro-oxidation of methanol.

The FTIR peak of Mo and Se are observed at 879 and 450 cm^{-1}. Furthermore, the Mo-Se vibrational peak is observed at 471 cm^{-1}. No peak is observed from 1700-2100 cm^{-1} shows the absence of carbonyl group after the electro-oxidation of methanol.

References

(1) Wang, X.; Xi, S.; Lee, W. S. V.; Huang, P.; Cui, P.; Zhao, L.; Hao, W.; Zhao, X.; Wang, Z.; Wu, H.; Wang, H.; Diao, C.; Borgna, A.; Du, Y.; Yu, Z. G.; Pennycook, S.; Xue, J. Materializing Efficient Methanol Oxidation via Electron Delocalization in Nickel Hydroxide Nanoribbon. *Nat Commun* **2020**, *11* (1), 4647. https://doi.org/10.1038/s41467-020-18459-9.

(2) Pecher, L.; Tonner, R. Deriving Bonding Concepts for Molecules, Surfaces, and Solids with Energy Decomposition Analysis for Extended Systems. *WIREs Computational Molecular Science* **2019**, *9* (4), e1401. https://doi.org/10.1002/wcms.1401.

(3) te Velde, G.; Baerends, E. J. Precise Density-Functional Method for Periodic Structures. *Phys. Rev. B* **1991**, *44* (15), 7888–7903. https://doi.org/10.1103/PhysRevB.44.7888.

(4) te Velde, G.; Bickelhaupt, F. M.; Baerends, E. J.; Fonseca Guerra, C.; van Gisbergen, S. J. A.; Snijders, J. G.; Ziegler, T. Chemistry with ADF. *Journal of Computational Chemistry* **2001**, *22* (9), 931–967. https://doi.org/10.1002/jcc.1056.

(5) Mulliken, R. S. Self-Consistent Field Atomic and Molecular Orbitals and Their Approximations as Linear Combinations of Slater-Type Orbitals. *Rev. Mod. Phys.* **1960**, *32* (2), 232–238. https://doi.org/10.1103/RevModPhys.32.232.

(6) Chen, Q.; Yang, Y.; Cao, Z.; Kuang, Q.; Du, G.; Jiang, Y.; Xie, Z.; Zheng, L. Excavated Cubic Platinum–Tin Alloy Nanocrystals Constructed from Ultrathin Nanosheets with Enhanced Electrocatalytic Activity. *Angewandte Chemie International Edition* **2016**, *55* (31), 9021–9025. https://doi.org/10.1002/anie.201602592.

(7) Fu, G.; Yan, X.; Cui, Z.; Sun, D.; Xu, L.; Tang, Y.; B. Goodenough, J.; Lee, J.-M. Catalytic Activities for Methanol Oxidation on Ultrathin CuPt 3 Wavy Nanowires with/without Smart Polymer. *Chemical Science* **2016**, *7* (8), 5414–5420. https://doi.org/10.1039/C6SC01501H.

(8) Lu, Q.; Sun, L.; Zhao, X.; Huang, J.; Han, C.; Yang, X. One-Pot Synthesis of Interconnected Pt95Co5 Nanowires with Enhanced Electrocatalytic Performance for Methanol Oxidation Reaction. *Nano Res.* **2018**, *11* (5), 2562–2572. https://doi.org/10.1007/s12274-017-1881-z.

(9) Qi, Z.; Xiao, C.; Liu, C.; Goh, T. W.; Zhou, L.; Maligal-Ganesh, R.; Pei, Y.; Li, X.; Curtiss, L. A.; Huang, W. Sub-4 Nm PtZn Intermetallic Nanoparticles for Enhanced Mass and Specific Activities in Catalytic Electrooxidation Reaction. *J. Am. Chem. Soc.* **2017**, *139* (13), 4762–4768. https://doi.org/10.1021/jacs.6b12780.

(10) Zheng, J.-N.; Li, S.-S.; Ma, X.; Chen, F.-Y.; Wang, A.-J.; Chen, J.-R.; Feng, J.-J. Popcorn-like PtAu Nanoparticles Supported on Reduced Graphene Oxide: Facile Synthesis and Catalytic Applications. *J. Mater. Chem. A* **2014**, *2* (22), 8386–8395. https://doi.org/10.1039/C4TA00857J.

(11) Wu, S.; Liu, J.; Tian, Z.; Cai, Y.; Ye, Y.; Yuan, Q.; Liang, C. Highly Dispersed Ultrafine Pt Nanoparticles on Reduced Graphene Oxide Nanosheets: In Situ Sacrificial Template Synthesis and Superior Electrocatalytic Performance for Methanol Oxidation.

ACS Appl. Mater. Interfaces **2015**, *7* (41), 22935–22940. https://doi.org/10.1021/acsami.5b06153.

(12) Yang, H.; Li, S.; Jin, R.; Yu, Z.; Yang, G.; Ma, J. Surface Engineering of Phosphorus Low-Doping Palladium Nanoalloys Anchored on the Three-Dimensional Nitrogen-Doped Graphene for Enhancing Ethanol Electroxidation. *Chemical Engineering Journal* **2020**, *389*, 124487. https://doi.org/10.1016/j.cej.2020.124487.

(13) Sadhukhan, M.; Kundu, M. K.; Bhowmik, T.; Barman, S. Highly Dispersed Platinum Nanoparticles on Graphitic Carbon Nitride: A Highly Active and Durable Electrocatalyst for Oxidation of Methanol, Formic Acid and Formaldehyde. *International Journal of Hydrogen Energy* **2017**, *42* (15), 9371–9383. https://doi.org/10.1016/j.ijhydene.2017.03.097.

(14) Zhang, F.; Wang, Z.; Xu, K. Q.; Xia, J.; Liu, Q.; Wang, Z. Highly Dispersed Ultrafine Pt Nanoparticles on Nickel-Cobalt Layered Double Hydroxide Nanoarray for Enhanced Electrocatalytic Methanol Oxidation. *International Journal of Hydrogen Energy* **2018**, *43* (33), 16302–16310. https://doi.org/10.1016/j.ijhydene.2018.07.059.

(15) Wang, H.; Chen, Y.; Xie, W.; Han, X.; Feng, Q.; Jiang, R.; Shang, H.; Zhang, F.; Gao, L.; Wang, Z. Construction of Highly Active Pt/Ni-Fe Layered Double Hydroxide Electrocatalyst towards Methanol Oxidation in Alkaline Medium. *International Journal of Electrochemical Science* **2019**, *14* (8), 7961–7972. https://doi.org/10.20964/2019.08.06.

(16) Sharma, M. D.; Mahala, C.; Basu, M. Nanosheets of MoSe2@M (M = Pd and Rh) Function as Widespread pH Tolerable Hydrogen Evolution Catalyst. *Journal of Colloid and Interface Science* **2019**, *534*, 131–141. https://doi.org/10.1016/j.jcis.2018.09.018.